Charlton TS, Rouainia M.

A probabilistic approach to the ultimate capacity of skirted foundationsin spatially variable clay.

***Structural Safety* 2017, 65, 126-136.**

A probabilistic approach to the ultimate capacity of skirted foundations in spatially variable clay

T.S. Charlton[1] and M. Rouainia[1]

[1]*School of Civil Engineering and Geosciences,Newcastle University, Newcastle NE1 7RU, UK*

Abstract

Skirted foundations are used in offshore applications to resist the large horizontal and moment loads that are characteristic of the ocean environment. The combination of vertical-horizontal-moment (VHM) loading results in complicated stress conditions in the seabed and design is often based on VHM failure envelopes. These have generally been constructed by numerical analysis using a deterministic characterisation of soil properties and disregard the natural spatial variability of marine sediments. In this study, spatial variability is taken into account by coupling a random field model with finite element analysis. The paper presents a probabilistic analysis of the ultimate capacity of skirted foundations in spatially variable undrained clay. The increase of strength with depth typical of a marine clay is included in the modelling framework. Probabilistic failure envelopes are constructed to analyse the effect of spatial variability when skirted foundations are subjected to different combinations of VHM loading. The results show that the probability of failure increases under high vertical loads and at peak moment capacity in the HM plane, suggesting that care should be taken in design at these areas of the failure envelope. The methodology demonstrates a straightforward and effective way of quantifying uncertainty in the ultimate limit state design of offshore geotechnical structures and the results presented provide specific guidance for the design of skirted foundations.

Keywords: Offshore geotechnics, skirted foundation, failure envelopes, spatial variability, finite element analysis

1. Introduction

In offshore applications, shallow foundations are often equipped with peripheral vertical skirts which penetrate into the seabed. The skirts improve the ability of the foundation to resist the large horizontal and moment loads that are imposed by environmental factors such as wind and waves. In undrained conditions, capacity may be enhanced by the development of suction within the enclosed soil plug which provides short term tensile resistance [11].

The interaction of vertical-horizontal-moment (VHM) loading, shown in Fig. 1, is a critical design issue. It has been shown that classical bearing capacity solutions are inadequate for describing the capacity of foundations in complex soil conditions subject to combined VHM loading, and often lead to under prediction of capacity [28, 14]. A far more versatile approach to assessing the ultimate limit state is to construct failure envelopes in VHM load space and compare design loads to those which would lead to failure of the foundation [27].

Numerical investigations of the shape of the undrained VHM failure envelope for skirted foundations with various embedment ratios and in uniform and normally consolidated clays have been undertaken by Yun and Bransby [7] and Gourvenec and Barnett [13]. These studies have considered the soil to be described by deterministic parameters following a defined trend. However, due to complex physical and chemical formation processes, soil is inherently a highly variable material and the values of engineering parameters can be observed to fluctuate through the soil mass [22]. Spatial variability is difficult to characterise in a deterministic model as knowledge of ground conditions is limited by constraints on site investigations, a particular factor offshore. Dealing with uncertainty is therefore a central component of geotechnical design.

Probabilistic studies using random fields to represent soil parameters have shown that spatial variability can affect both the failure mechanism and bearing capacity of surface footings [15, 25, 1]. VHM failure envelopes for a surface footing on spatially variable clay have also been constructed by Cassidy et al. [8]. Footing embedment has been considered in a recent study by Pieczyńska-Kozłowska et al. [23] of bearing capacity on a spatially variable drained soil. However, for skirted foundations the relatively low embedment ratio, defined by the ratio D/B as shown in Fig. 1, means that the soil plug must be taken into account in the determination of the VHM failure envelope and substitution of a solid embedded foundation at the same depth may be inappropriate [7]. In addition, marine clays are characterised by an increasing strength with depth [27], the gradient of which can significantly influence footing behaviour [14]. In general, previous probabilistic investigations of surface footings have considered a uniform soil mass with strength constant with depth, which may not be applicable in the offshore environment.

In this paper, the ultimate capacity of skirted foundations in spatially variable undrained clay is assessed under both uniaxial loading and combinations of VHM loads. Probabilistic failure envelopes are constructed to illustrate the effect of combined loading on the probability distribution of bearing capacity under different load combinations. The probabilistic envelopes are based upon cumulative distribution functions (CDFs), and enable a better understanding of the level of risk associated with this appealing design methodology. In addition, this study incorporates the increase of strength with depth that is typical of marine clays and an important consideration in offshore applications.

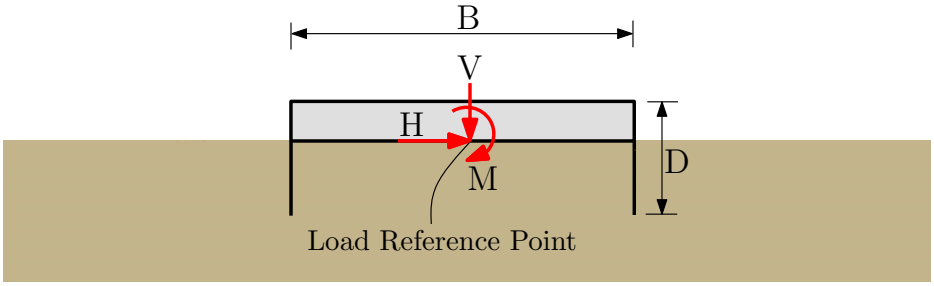

Figure 1: VHM loading of a skirted foundation.

2. Computational framework

The effect of spatial variability on the undrained VHM capacity of skirted foundations is assessed by coupling a random field model with finite element (FE) analysis. Monte Carlo simulation is used to characterise the stochastic response, i.e. the probability density function (PDF) of ultimate capacity. The implementation is non-intrusive, meaning the FE code is not modified and proceeds in the usual deterministic manner. In each simulation, a random field is generated and passed to the FE solver, where the VHM capacity is obtained.

2.1. Simulation of spatial variability

The undrained shear strength, s_u, is generally used to determine bearing capacity in undrained conditions. A correlated random field of s_u will therefore be considered in order to simulate the spatial variability that would likely occur in the field.

Marine sediments are often normally consolidated and exhibit an increasing strength with depth. This creates an additional challenge for simulating spatial variability as the random field can no longer be homogeneous, whereby the joint PDF of the random field is constant across the domain [29]. An assumption of homogeneity greatly simplifies the treatment of random fields; in the case of a Gaussian random field, only the mean and variance are needed to define

the entire field. However, the undrained shear strength may be related to the overconsolidation ratio (OCR) and effective vertical stress, σ'_v, as follows [30]:

$$\frac{s_u}{\sigma'_v} = rOCR^m \tag{1}$$

where r and m are constants. In a normally consolidated marine clay, OCR is equal to 1. If a limited mudline strength, $s_{u,m}$, is accounted for, the profile of s_u increasing with depth may be expressed as:

$$s_u = r\sigma'_v + s_{u,m} = r\gamma' z + s_{u,m} \tag{2}$$

where z is the depth below the mudline and γ' the effective unit weight of the clay. Spatial variability may therefore be taken into account by considering r as a homogeneous random field [19]. Here, both γ' and $s_{u,m}$ are taken as deterministic quantities.

The mean (μ_{s_u}) and standard deviation (σ_{s_u}) of s_u are:

$$\mu_{s_u} = s_{u,m} + \gamma' z \mu_r \tag{3}$$

$$\sigma_{s_u} = \gamma' z \sigma_r \tag{4}$$

where μ_r and σ_r are the mean and standard deviation of r, respectively. Both μ_{s_u} and σ_{s_u} are dependent upon the vertical effective stress. The increase in variability of s_u with depth has been observed by Lumb [20] in a normally consolidated marine clay and so can be considered to represent a typical offshore scenario.

It is clear that s_u should not be a negative value and a Gaussian distribution would therefore be unsuitable for r. A lognormal distribution takes only positive values, making it an appropriate choice. If $\mathbf{x}$ denotes spatial position, the lognormal random fields $r(\mathbf{x})$ and $s_u(\mathbf{x})$ can be generated by:

$$r(\mathbf{x}) = \exp\left[\mu_{L,r} + \sigma_{L,r} G(\mathbf{x})\right] \tag{5}$$

$$s_u(\mathbf{x}) = s_{u,m} + \gamma' z r(\mathbf{x}) \tag{6}$$

where $G(\mathbf{x})$ is a standard homogeneous Gaussian random field of zero mean and unit variance and $\mu_{L,r}$ and $\sigma_{L,r}$ are, respectively, the mean and standard deviation of $\ln(r)$.

The standard Gaussian random field $G(\mathbf{x})$ is generated using the Karhunen-Loeve (KL) expansion. Keaveny et al. [17] analysed the correlation structure of s_u at several offshore sites and found that an exponential autocorrelation function can provide a suitable fit. This is convenient from a numerical perspective as analytical solutions of the KL eigenvalue problem are available for this type of autocorrelation function [10]. Here, an anisotropic exponential autocorrelation function is used. The autocorrelation distances in x- and y-directions (L_x, L_y) of the transformed field $s_u(\mathbf{x})$ are comparable to those of $r(\mathbf{x})$ [31]. The values of L_x and L_y of $\ln(r)$ are taken to be 10m (2.5×B) and 1m (0.25×B) respectively, consistent with reported values in literature [e.g. 18, 22].

The random field is discretised on a rectangular grid, referred to as the stochastic mesh, which is separate from the FE mesh but defined on the same geometry. The coupling between the random field and FE model is achieved by interpolating the values of the random field on the stochastic mesh to the Gauss points of the FE mesh using shape functions. Note that this means that while $s_{u,m}$ is deterministic when generating the random field, in the finite element model the mudline strength will be random due to interpolation from the stochastic mesh.

2.2. Finite element model

The deterministic simulations are carried out using the commercial FE code Plaxis 2D [24]. A range of embedment ratios between 0 and 1 were considered in order to observe the effect of skirt length on the ultimate capacity of the foundation. Plane strain analysis was used to minimise computation time and allow comparison with previous FE studies. It has also been found that the VHM failure envelope of plane strain and circular surface footings is very similar [11], but further investigation would be required to generalise the results presented here.

The clay is assumed to be undrained and obeys a linear elastic-perfectly plastic Mohr-Coulomb constitutive law, which is equivalent to the Tresca criterion in undrained conditions. In the deterministic case the undrained shear strength of the clay increases with depth according to $s_u = s_{u,m} + kz$ where k is the increase in s_u per metre depth. A dimensionless parameter, κ, may be used to describe the degree of heterogeneity with $\kappa = kB/s_{u,m}$ [13]. A value of κ = 2 was chosen, which corresponds to a fairly typical heterogeneity observed for offshore sediments [e.g. 2]. The effective unit weight is taken as 10kN/m^3. In the stochastic case, the mean of s_u is derived from $\mu_r = k/\gamma'$ and the coefficient of variation (COV) of r is chosen to be 0.2 based on values of the variability of s_u reported in Lacasse and Nadim [18]. It should be noted that

COV_{s_u} increases towards COV_r with depth as, following Li et al., [19], the quantities are related by:

$$COV_{s_u} = \frac{COV_r \mu_r \gamma'}{\mu_r \gamma' + s_{u,m}/z} \tag{7}$$

A typical FE mesh, consisting of 15-node triangular elements, is shown in Fig. 2 for an embedment ratio of 0.25; a similar level of mesh refinement was used for all embedment ratios. The model boundaries are located sufficiently distant to have no effect on the results. Due to the large number of simulations that must be completed, a balance must be found between calculation time and solution accuracy with regards to mesh discretisation. For the example case with D/B = 0.25, a mesh of 666 elements was found to overestimate uniaxial capacity by no more than 2.5% compared with a mesh of over 2700 elements; this was viewed as acceptable keeping in mind the savings in calculation time.

The skirted foundation is modelled using rigid plate elements. Interfaces are applied along the vertical skirt with extensions beyond the skirt tip to avoid unrealistic stress concentrations. It is assumed that suction is generated in the clay plug during loading, thus no reduction in strength is considered between the foundation and soil. Installation effects on the outside wall of the skirt are also neglected.

A load-controlled method is used to define the VHM envelopes. Load probes at different angles, corresponding to fixed ratios of VH, VM and HM loads, are applied at the load reference point (defined in Fig. 1) until failure. The load probes are regularly spaced at 15^o increments, as shown in Fig. 3. The failure envelope is subsequently constructed from the defined failure points. Note that in certain cases additional load probes were used to capture significant points on the envelope.

3. Results and discussion

The increase of s_u with depth is illustrated in Fig. 4. The deterministic profile of s_u corresponds to the mean of the stochastic cases. Three realisations of a vertical cross section from different random fields are shown and the increase in variability of s_u at greater depths can be clearly observed. An example of a random field is shown in Fig. 5. The autocorrelation distance in the x-direction is an order of magnitude greater than in the y-direction, resulting in horizontal bands of stronger and weaker soil.

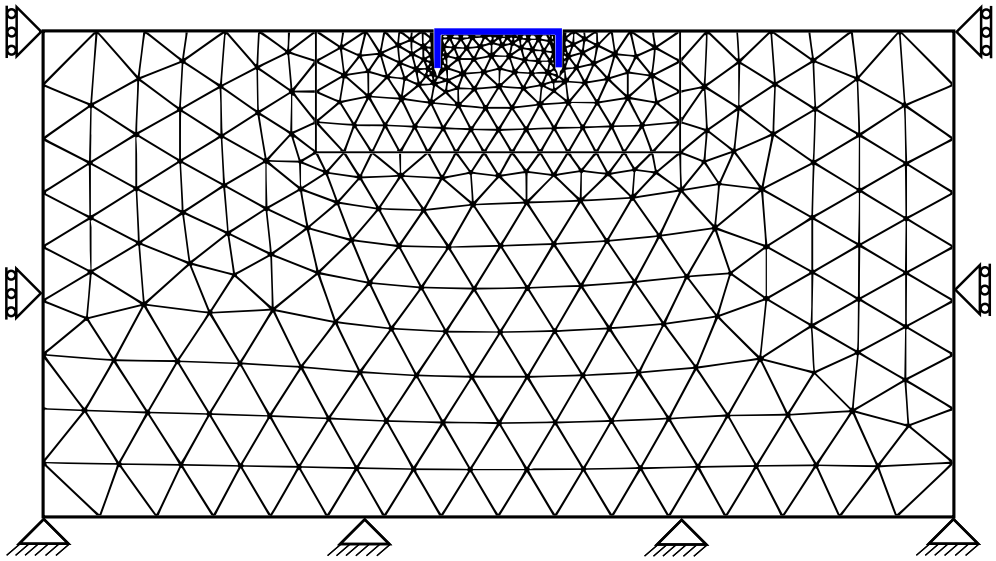

Figure 2: Typical finite element mesh (D/B = 0.25).

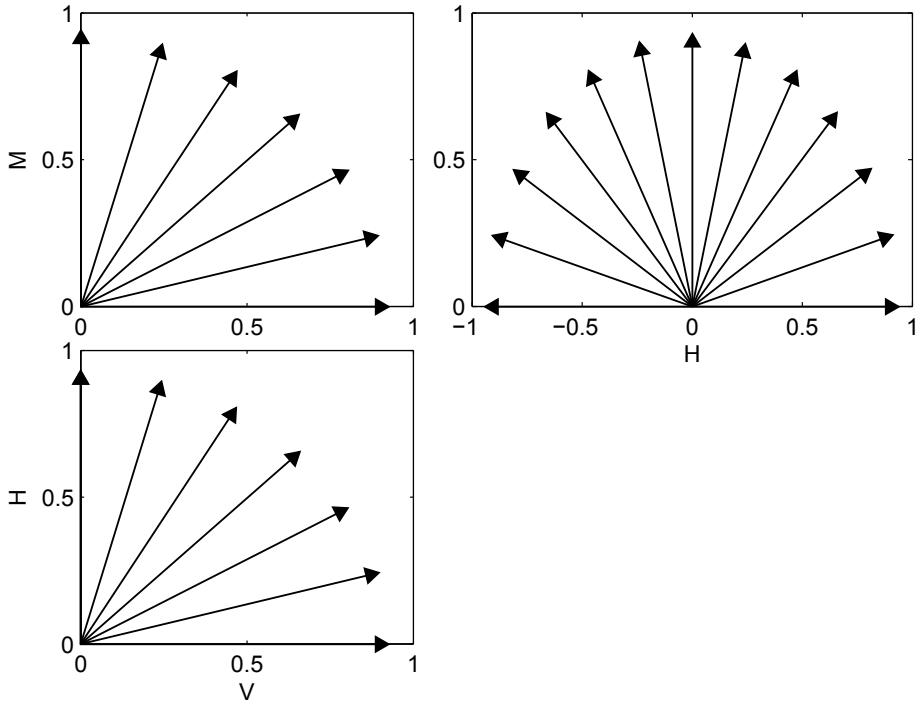

Figure 3: Load probes used to define VHM failure envelopes.

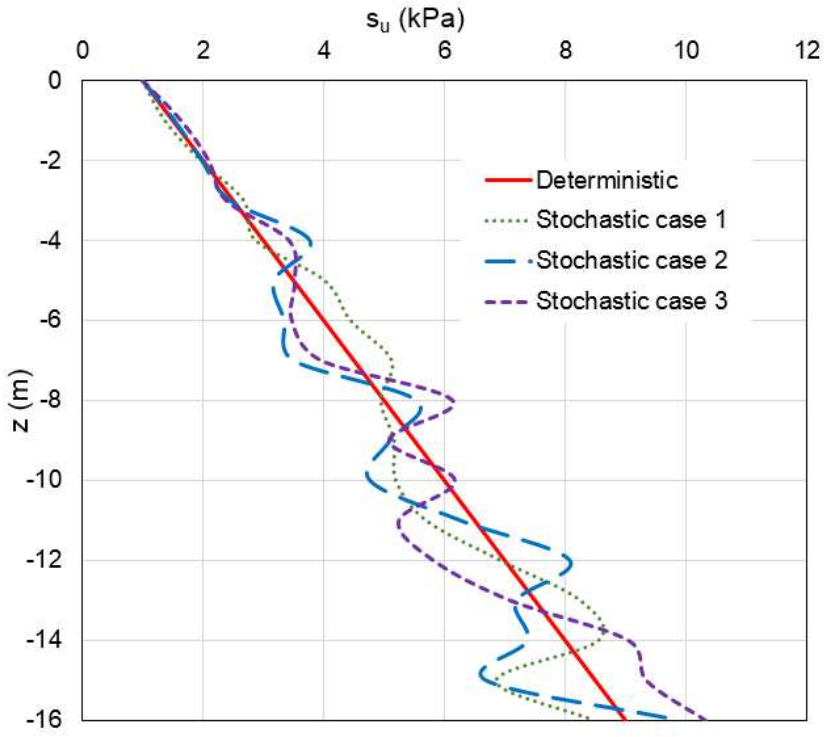

Figure 4: Increase of s_u with depth, showing the deterministic profile and 3 stochastic cases.

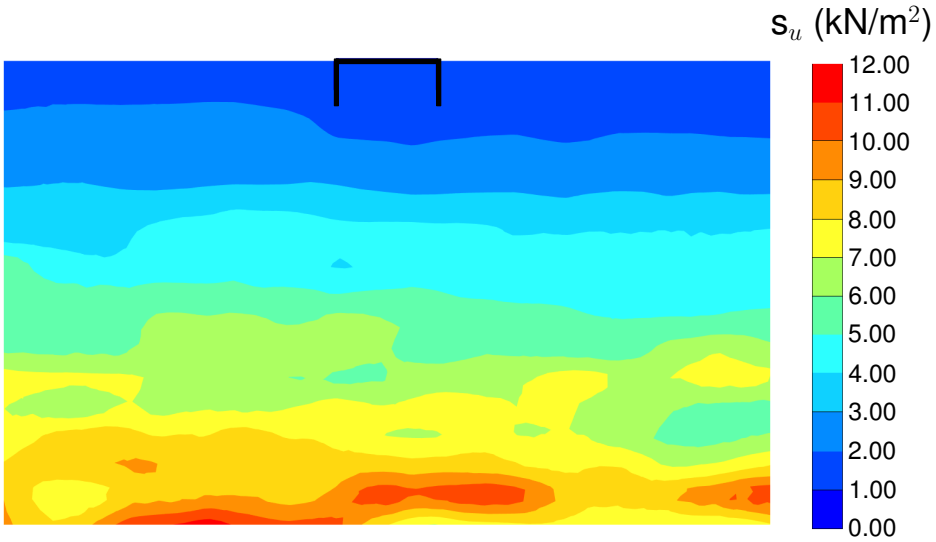

Figure 5: Realisation of a random field of s_u.

3.1. Uniaxial capacity

As a reference case, 1000 Monte Carlo simulations were used to determine the stochastic response of a skirted foundation with an embedment ratio of 0.25. Fig. 6 shows the evolution of the mean and COV of the uniaxial capacities, denoted V_0, H_0 and M_0 and referring to pure vertical, horizontal and moment loading respectively, throughout the Monte Carlo simulations. The mean is normalised by the respective uniaxial deterministic capacities to facilitate comparison (i.e. $\mu = \mu_Q/Q_{Det}$ if Q is the ultimate capacity for a given load probe). It can be seen that both statistics converge to an approximately constant value. Similar convergence was observed for higher moments (skewness and kurtosis), indicating that the response PDF of each load probe has been well captured. In view of this convergence and the computational time involved, which could be over an hour for one simulation of D/B=1 for example, 500 simulations were used to characterise the stochastic response for other embedment ratios.

The results of the uniaxial loading cases from stochastic and deterministic analyses are presented in Table 1. Results are given in terms of dimensionless capacity factors defined by: $N_{c,V} = V/Bs_{u,tip}$, $N_{c,H} = H/Bs_{u,tip}$, and $N_{c,M} = M/B^2_{s_{u,tip}}$. For comparison purposes, the reference value of undrained shear strength, $s_{u,tip}$, is taken at skirt tip level. In the stochastic case this corresponds to the prescribed mean value of s_u at that depth, which is equal to the deterministic value. Confidence intervals are constructed by bootstrap resampling [9]; 10,000 samples with replacement were drawn from the observations and a 95% confidence interval estimated from the empirical distribution.

Firstly, it can be seen that the deterministic FE analysis in this study predicts bearing capacity factors 5-10% less than those reported by Gourvenec and Barnett [13]. The horizontal capacity factor for a surface footing, the case where no vertical skirts are present and the embedment ratio is 0, is independent of the shear strength heterogeneity, described by κ, and should theoretically be equal to 1 if failure occurs by sliding. The overestimate in the current FE analysis is approximately 7%, which may be attributed to the level of mesh refinement.

The mean of each uniaxial capacity factor tends to be very similar to the corresponding deterministic value, differing by no more than $\pm$ 3% for all loads and embedment ratios. The statistics are closely bracketed by the 95% confidence intervals, indicating the certainty that may be placed in the reported results.

The effect of embedment ratio on the COV of the uniaxial capacity factors is shown in Fig. 7. Examples of the failure mechanisms under uniaxial loading for 3 different random field realisations, with D/B = 0, 0.5 and 1, are presented in Fig. 8. For a surface footing the gov-

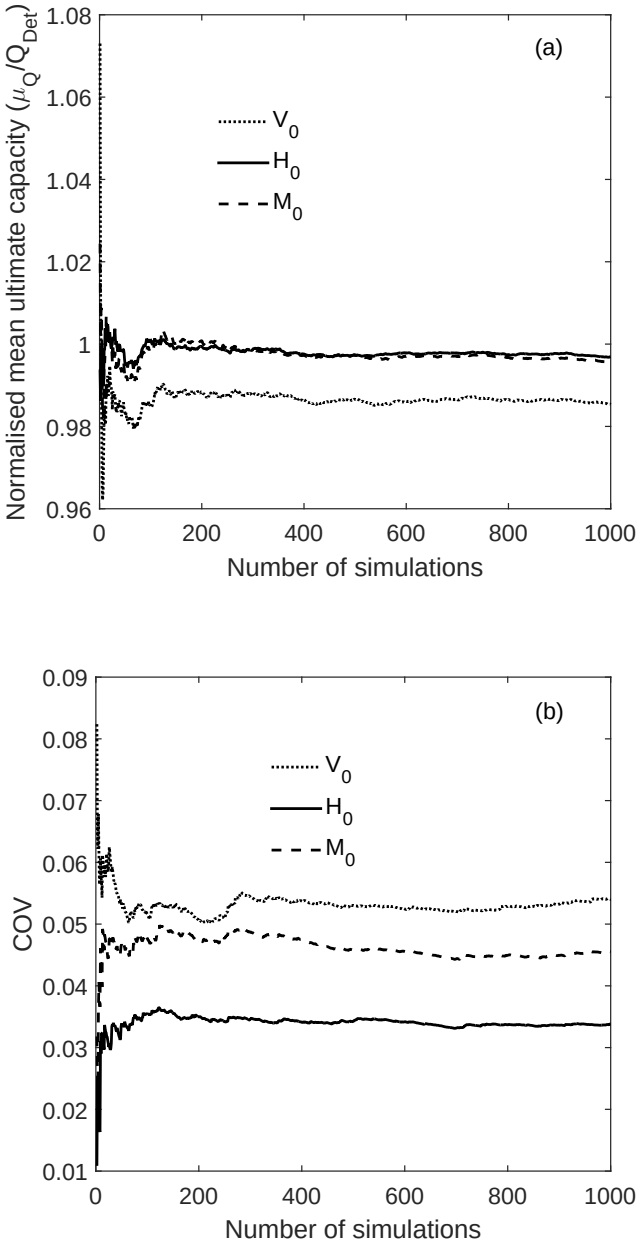

Figure 6: (a) Normalised mean of uniaxial capacities and (b) COV of uniaxial capacities as a function of the number of Monte Carlo simulations for D/B = 0.25.

Table 1: Stochastic and deterministic uniaxial capacity factors. For stochastic analyses, 95% confidence intervals (CI) of mean (μ) and standard deviation (σ) are shown. (*Approximate values from Fig. 3 in Gourvenec and Barnett [13])

D/B	Capacity factor	μ	95% CI	σ	95% CI	COV	Deterministic	Gourvenec and Barnett [13]*
0	$V_0/B_{s_{u,tip}}$	7.689	(7.666,7.713)	0.272	(0.254,0.295)	0.035	7.677	8.06
	$H_0/B_{s_{u,tip}}$	1.072	(1.072,1.073)	0.005	(0.005,0.005)	0.005	1.074	1.07
	$M_0/B^2_{s_{u,tip}}$	1.008	(1.004,1.012)	0.045	(0.042,0.049)	0.044	1.009	1.04
0.25	$V_0/B_{s_{u,tip}}$	8.464	(8.502,8.550)	0.457	(0.374,0.410)	0.054	8.591	9.02
	$H_0/B_{s_{u,tip}}$	2.052	(2.046,2.054)	0.069	(0.061,0.067)	0.031	2.051	2.15
	$M_0/B2_{s_{u,tip}}$	1.033	(1.031,1.036)	0.047	(0.038,0.041)	0.046	1.035	1.14
0.50	$V_0/B_{s_{u,tip}}$	8.790	(8.744,8.834)	0.518	(0.488,0.549)	0.059	8.980	9.35
	$H_0/B_{s_{u,tip}}$	2.530	(2.522,2.539)	0.098	(0.093,0.105)	0.039	2.509	2.70
	$M_0/B^2_{s_{u,tip}}$	1.211	(1.206,1.216)	0.056	(0.053,0.060)	0.046	1.176	1.30
1	$V_0/B_{s_{u,tip}}$	9.389	(9.340,9.438)	0.554	(0.520,0.597)	0.059	9.589	9.90
	$M_0/B_{s_{u,tip}}$	2.742	(2.731,2.753)	0.125	(0.118,0.134)	0.046	2.746	3.37
	$M_0/B^2_{s_{u,tip}}$	1.927	(1.916,1.938)	0.126	(0.119,0.135)	0.065	1.922	2.02

erning failure mechanism under pure horizontal loading is sliding, as evident in Fig. 8(a). The undrained shear strength at the mudline therefore determines the ultimate capacity, resulting in a very low COV of 0.005 as the values of s_u at the Gauss points closest to the surface show little variability.

For both horizontal and vertical loading, the variability of the response increases considerably once vertical skirts are added to the foundation. Recalling that the standard deviation of s_u increases with depth, this is due to the skirts transferring the failure mechanism into deeper, and consequently more variable soil. However, the rate of increase in COV reduces as skirt length is increased from D/B = 0.25 to 1. Under vertical loading, there is in fact no change in COV between an embedment ratio of 0.5 and 1. From Figs. 8(b) and (c) it can be seen that the mode of failure is the same in the two cases. It might be expected that the deeper mechanism for D/B = 1 would lead to a higher COV, but the longer shear planes appear to have a spatial averaging effect on the response, reducing the influence of individual zones of stronger and weaker clay. The COV of the ultimate capacity, under any combination of loads, is a result of the combined influence of spatial variability and the form of the failure mechanism.

Under horizontal loading the shear planes do not extend below the skirt tips, except in the case of D/B = 1, shown in Fig. 8(c), where a limited rotational shear plane develops between the skirt tips. In general, a deeper mechanism forms under vertical loading. In the deterministic case the shear planes on either side of the foundation are equal in length but the spatial variation of s_u causes an asymmetric mechanism, which is clearly visible in Fig. 8. This results in higher values of COV across all embedment ratios for vertical loading.

Subjected to a pure moment, the variability of the ultimate capacity is relatively consistent from D/B = 0 to 0.5, with a COV of approximately 0.045. This is in contrast to the clear increase in COV observed under vertical and horizontal loading when skirts are added to the foundation. Instead, in the case of a moment load an increase in variability is observed when the embedment ratio is greater than 0.5, with COV equal to 0.065 at D/B = 1. Again, this can be related to the failure mechanism. Figs. 8(a) and (b) show that for D/B $\leq$ 0.5, the centre of rotation of the foundation is located at or above the load reference point and so forms a similar 'scoop' mechanism [6] in each case. However, as demonstrated in Fig. 8(c), when D/B = 1 the centre of rotation is located beneath the load reference point, at a depth approximately equal to half the skirt length. This 'scoop-slide' mechanism, identified by Yun and Bransby [32], is deeper and leads to a more variable response.

A description of the stochastic response of skirted foundations in terms of second order statistics is useful to identify differences in variability under different loading scenarios. However,

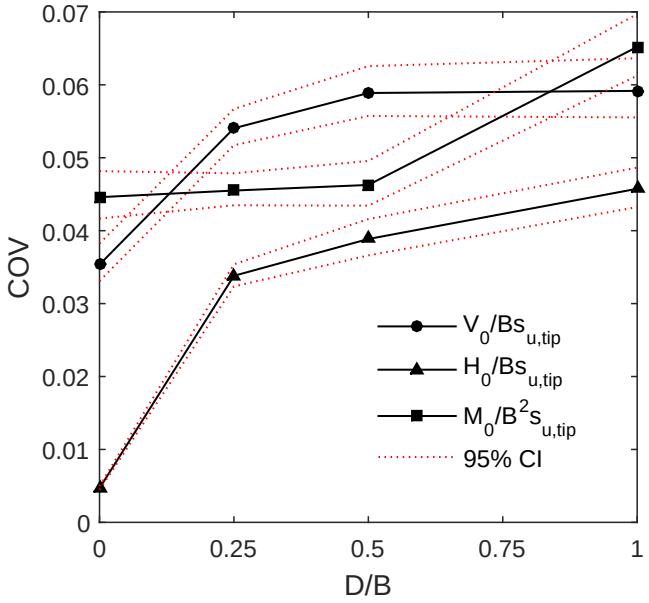

Figure 7: COV for uniaxial capacity factors at different embedment ratios.

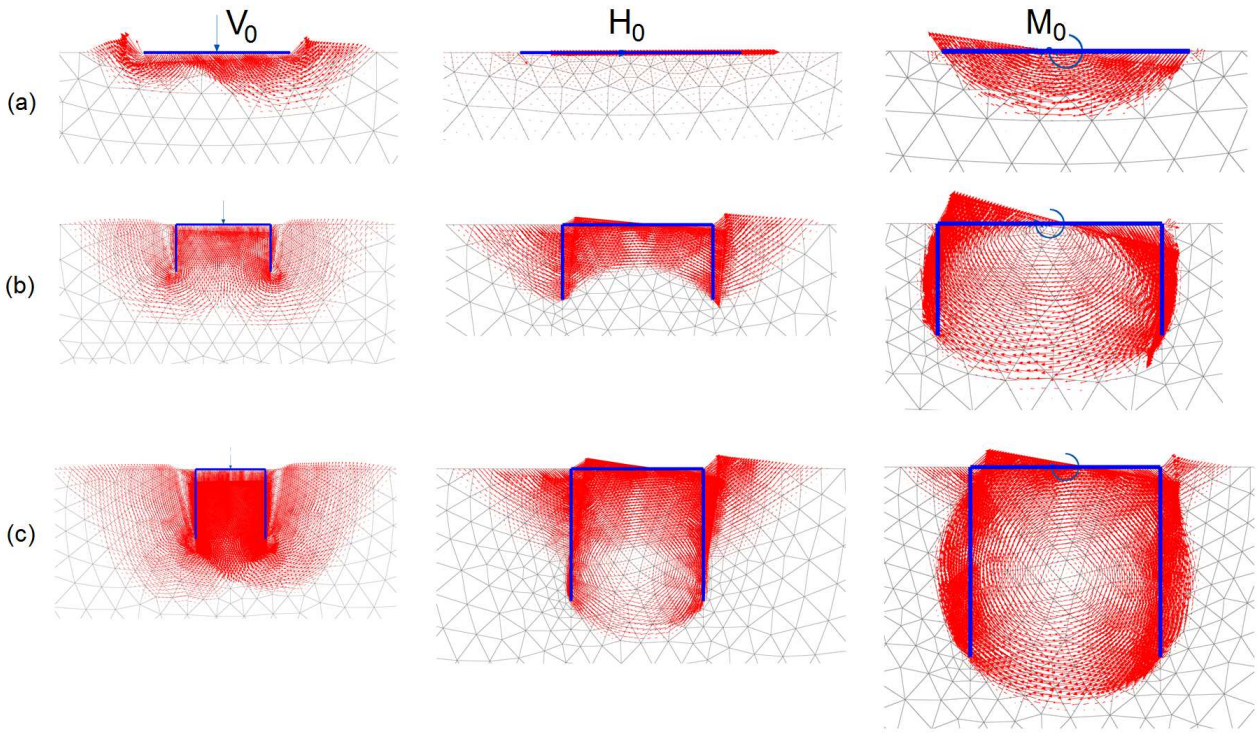

Figure 8: Vectors of incremental displacement at failure under uniaxial loading for (a) D/B = 0, (b) D/B = 0.5 and (c) D/B =1; (a) - (c) correspond to different random field realisations.

for design purposes the full range of the response is of interest. The coupled random field-FE methodology implemented in this study allows samples to be drawn from the unknown PDF of the ultimate capacity. The CDF can then be used to obtain probabilistic capacity factors, $N_{c,p}$, that correspond to a given probability, p, that the actual bearing capacity of the foundation will be less than or equal to $N_{c,p}$. With the CDF of the capacity factor denoted by F_{N_c}, $N_{c,p}$ is obtained by:

$$p = F_{N_c}(N_{c,p}) = P(N_c \leq N_{c,p}) \tag{8}$$

$$N_{c,p} = F_{N_c}^{-1}(p) \tag{9}$$

Inverting the CDF to obtain a unique value, as required by Eq. 9, is only possible if F is a strictly increasing function. This is not satisfied by the empirical CDF. Particularly at the tails of the distribution, which are likely to be of practical interest, the sparse number of samples result in a coarse approximation of the underlying 'true' distribution. This is a well-known drawback of Monte Carlo simulation and, although outside the scope of this study, more advanced methods such as subset simulation [3] or polynomial chaos expansions [4] could be applied. Here, kernel density estimation (KDE) is used to produce a smooth function that can be easily inverted and can better approximate the tails of the distribution, as evident in Fig. 9. A non-parametric technique is applied to avoid the need to assume a certain form of probability distribution, which is useful when considering the whole series of load probes. The robust and optimal KDE method proposed by Botev et al. [5] is used to estimate the CDF. As no closed-form expression is available, values of the CDF are evaluated on a fine grid (at 4096 points) and interpolation used to solve Eq. (9).

Fig. 10 shows the probabilistic bearing capacity factors as a function of embedment ratio. As the probabilistic factors are defined by inverting the CDF, the interpretation is clear. For example, the 1% probabilistic capacity factor, $N_{c,1}$, is defined as being the bearing capacity factor at which there is a probability of 1% that the random variable N_c, the actual bearing capacity factor, will be less than or equal to $N_{c,1}$, i.e. $P(N_c \leq N_{c,1}) = 0.01$. The figure shows that the distribution of the vertical bearing capacity factor has the greatest spread, a result of the relatively larger standard deviation. However, it is notable that despite $N_{c,V}$ having the same COV at D/B = 0.5 and 1, the tail of the distribution, (represented by $N_{c,0.1}$) is more extreme at the deeper embedment ratio relative to the position of the median ($N_{c,50}$).

For each loading scenario, the deterministic capacity factor ($N_{c,det}$) is close to, or above,

$N_{c,50}$. There is consequently a probability of 50% or greater that the ultimate capacity of the foundation will be less than that predicted by a deterministic analysis; this is often referred to as the probability of failure $P_f = P(N_c \leq N_{c,det})$ (e.g. Griffiths and Fenton [15]. The ISO design code for offshore structures [16] takes a classical bearing capacity approach to the ultimate limit state and recommends applying a partial factor of safety, FS, of 1.25 to the undrained shear strength. If this factor of safety is lumped into the bearing capacity factor, such that $N_{c,FS} = N_{c,det}/FS$, it can be seen that the probability of failure with respect to $N_{c,FS}$, denoted $P_{f,FS}$, is less than 0.1% ($= 10^{-3}$). The only exception is under vertical loading, where $P_{f,FS}$ marginally exceeds 10^{-3} at D/B = 1. This suggests that the current factor of safety is likely to be sufficient to account for the spatial variability of s_u in this scenario.

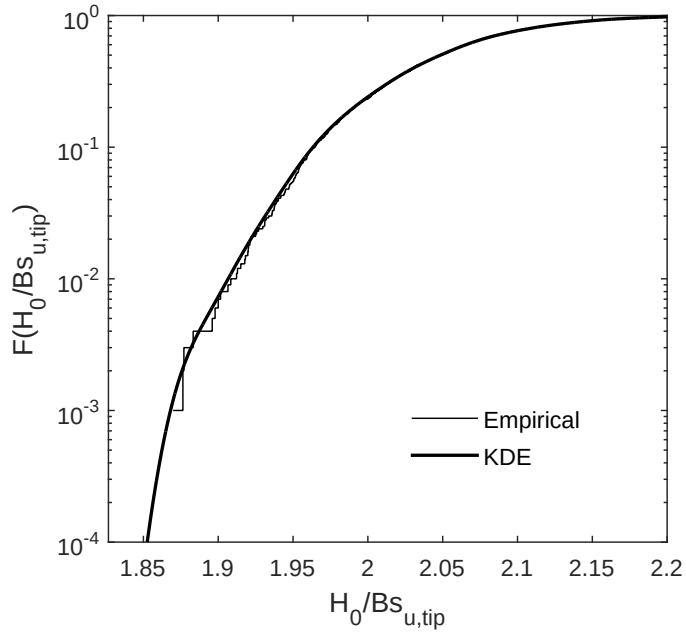

Figure 9: CDF of horizontal bearing capacity factor (D/B = 0.25).

3.2. Probabilistic VHM failure envelopes

The failure envelopes from each Monte Carlo simulation for the reference case (D/B = 0.25) are shown in Fig. 11, in addition to the deterministic envelopes. Consideration of the spatial variability of s_u has the potential to result in significant divergence of the failure envelope from the deterministic solution. It is also apparent that the variability is not constant around the failure envelope and so cannot be characterised from the uniaxial capacities alone. For the VH and VM envelopes, the stochastic capacity can vary up to $\pm$ 20% of the deterministic. In the HM plane, the probability distribution of the response is irregular. There is greater variability

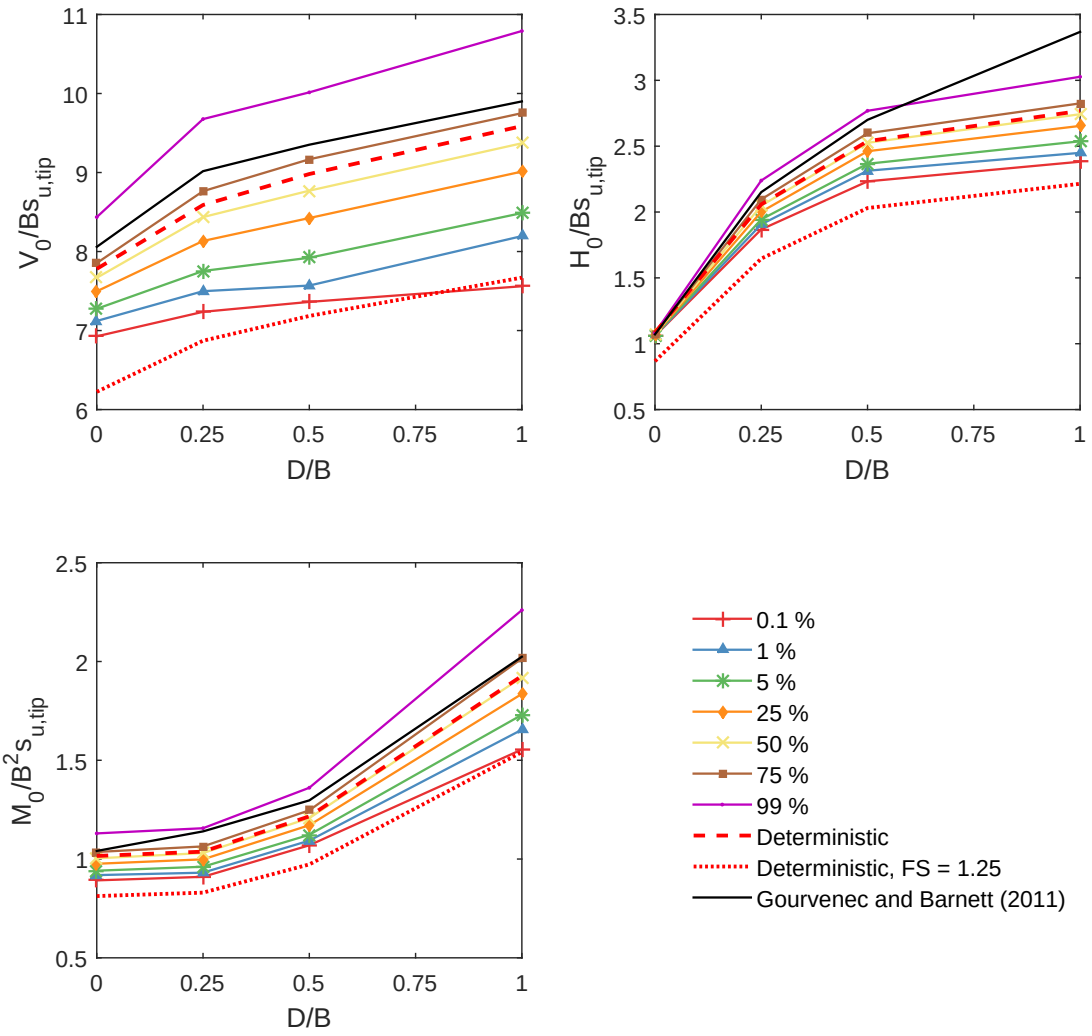

Figure 10: Probabilistic and deterministic uniaxial capacity factors for vertical, horizontal and moment loading.

for combinations of negative horizontal load and moment than for positive horizontal loads, and the greatest spread of potential capacity occurs at peak moment capacity.

While it is clear from Fig. 11 that consideration of spatial variability has the potential to affect the size and shape of the failure envelopes, it would be useful to quantify this variability in capacity in order assess the effect of spatial variability on the failure envelope design method. This can be achieved using the same method as for the uniaxial capacities. In order to construct probabilistic failure envelopes, first recall that the Monte Carlo procedure to define the envelopes used a series of n load probes of fixed direction. The ultimate capacity in each direction is a random variable. Then, if $\boldsymbol{N_c}$ is the collection of random variables N_c^i that define the VHM envelopes, with $i = 1, \ldots, n$, the probabilistic failure envelope corresponding to the probability p is denoted $\boldsymbol{N_{c,p}}$ and can be constructed componentwise as before:

$$N_{c,p}^i = F_{N_c^i}^{-1}(p) \tag{10}$$

where $F_{N_c^i}$ is the CDF of the ith load probe. The envelopes are constructed using KDE, as discussed previously, in order to obtain an invertible CDF. Cassidy et al. [8] constructed probabilistic failure envelopes using an empirical estimate of the probability of occurrence of a group of failure points based upon the distance from the origin. The approach followed here may produce a more accurate probabilistic failure envelope since, as evident in Fig. 11, the probability distribution of the capacity is not constant and so the shape of the CDF can change around the envelope.

Figs. 12 to 15 show the probabilistic failure envelopes for embedment ratios 0, 0.25, 0.5 and 1. Similar to the uniaxial capacities, in each case the $\boldsymbol{N_{c,50}}$ envelope is very close to the deterministic ($P_f \approx 0.5$). A consideration of the spatial variability of s_u in the failure envelope design process is therefore important. An appropriate factor of safety should be used to account for the uncertainty in s_u; here, the same factor of safety (FS = 1.25) is applied as for the uniaxial capacities in order to observe how load interaction affects the probability of failure.

As shown in Fig. 12, for a surface footing there is little difference between the probabilistic and deterministic envelopes when loading is dominated by a horizontal force. As discussed previously, this is a result of the assumptions made about the increase of s_u with depth and the shallow sliding mechanism that governs failure in this loading scenario. Significantly more variability occurs in the VM and HM planes, evident by the divergence of the probabilistic and deterministic envelopes. In the HM plane, there is a good fit between the deterministic envelope from the FE analysis in this study and that undertaken by Gourvenec and Barnett [13].

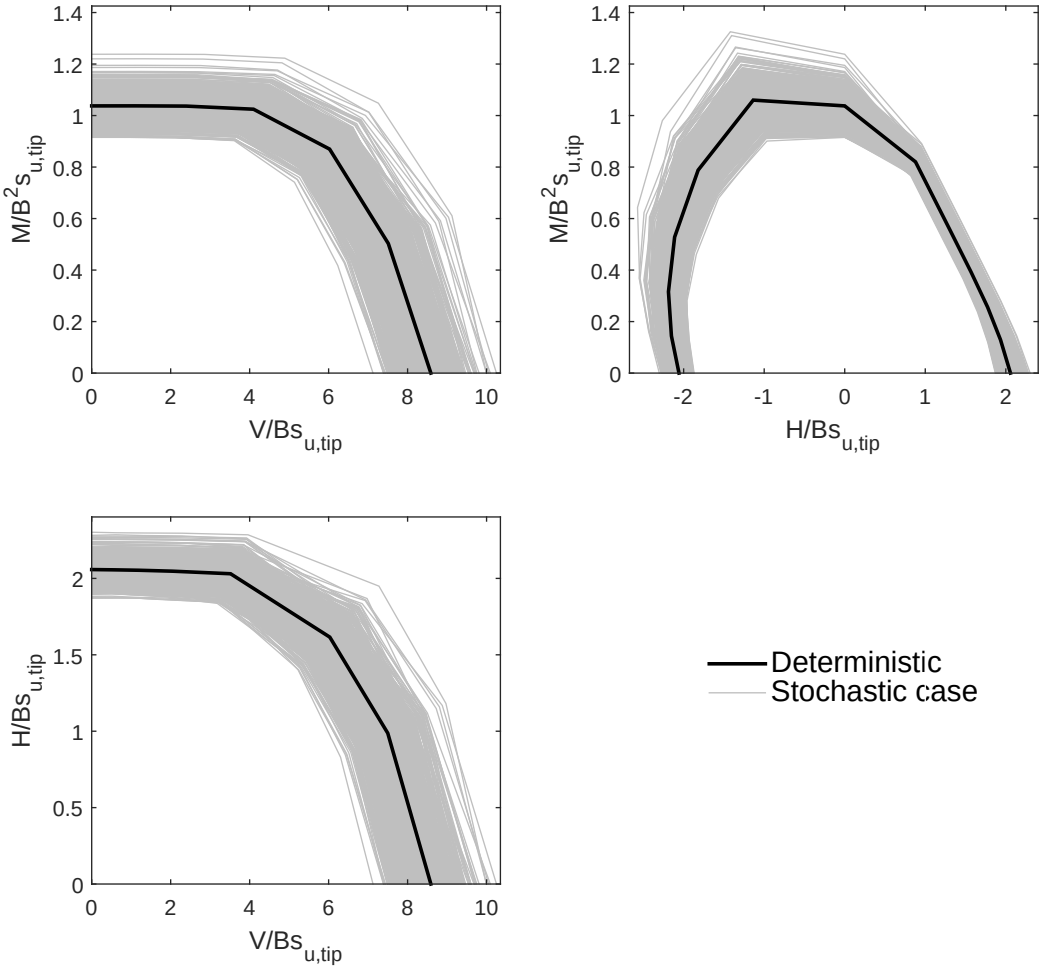

Figure 11: Stochastic and deterministic VHM failure envelopes.

In this plane, under positive horizontal load the probabilistic envelopes begin to diverge from the deterministic when the spatial variability of the soil influences the transition from pure sliding, visible as a vertical section of the envelope, to a rotational failure mechanism. Notice that initially this only affects the 0.1% and 1% envelopes, suggesting a reduction in capacity from a pure sliding mechanism with certain spatial distributions of undrained shear strength. The peak moment capacity shows a high variability due to the predominately rotational mechanism.

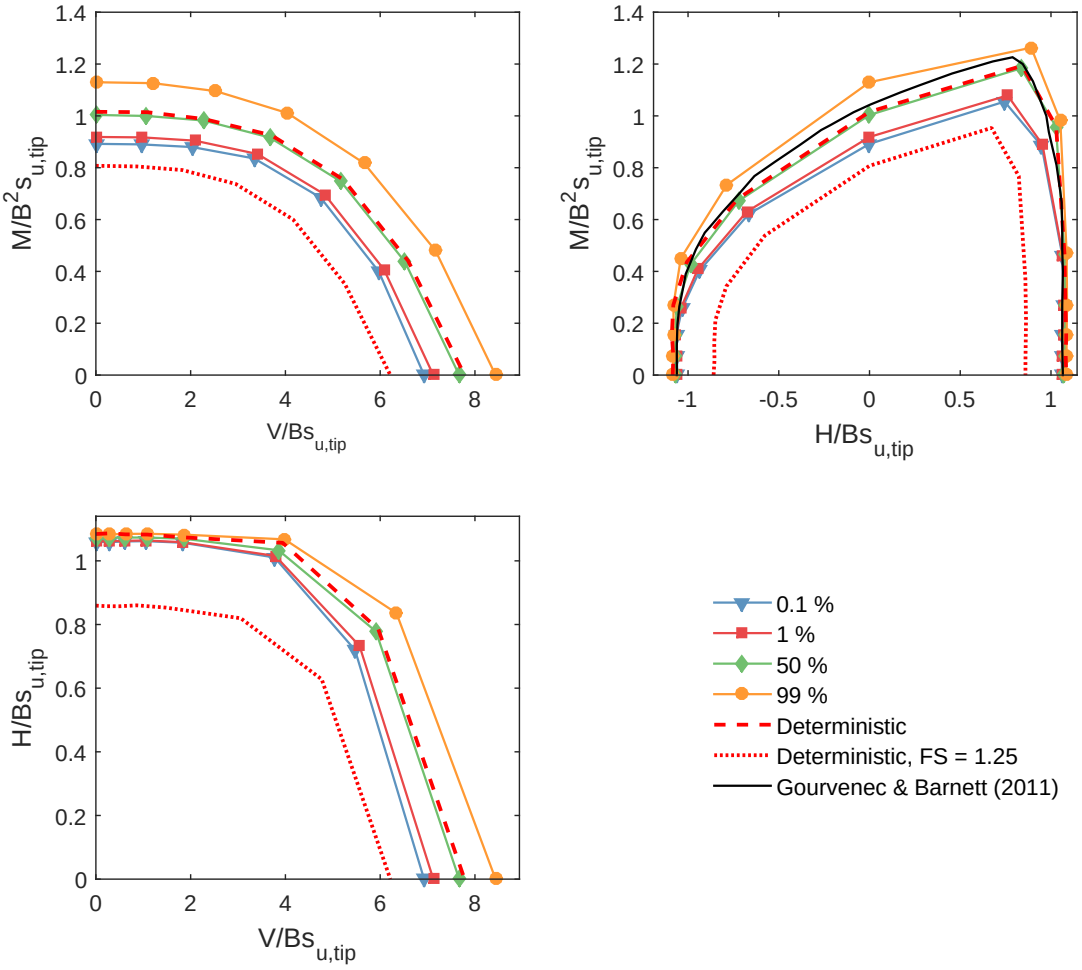

Figure 12: Probabilistic VHM failure envelopes for D/B = 0.

When vertical skirts are added to the foundation, the failure envelope in the HM plane becomes increasingly eccentric. This has been observed by many researchers, for example Gourvenec and Barnett [13] and, for the analogous case of embedded foundations, by Yun and Bransby [32], Gourvenec[12] and Bransby and Yun [7]. The choice of load reference point in this study, at the centre of the foundation for all embedment ratios, results in the eccentricity of the envelope reversing direction from a rightwards 'lean' at D/B = 0 (Fig. 12) to a leftwards 'lean' for footings with vertical skirts (Figs. 13 to 15). The response of the foundation is most

variable close to the peak moment capacity. This is particularly evident in Fig. 15 for D/B = 1, where the 1% and 99% envelopes at peak moment capacity are ± 15% of the deterministic. It can also be seen that the probability of failure, P_f^{FS} increases at peak moment capacity, approaching the $\boldsymbol{N}_{\boldsymbol{c},0.1}$ envelope.

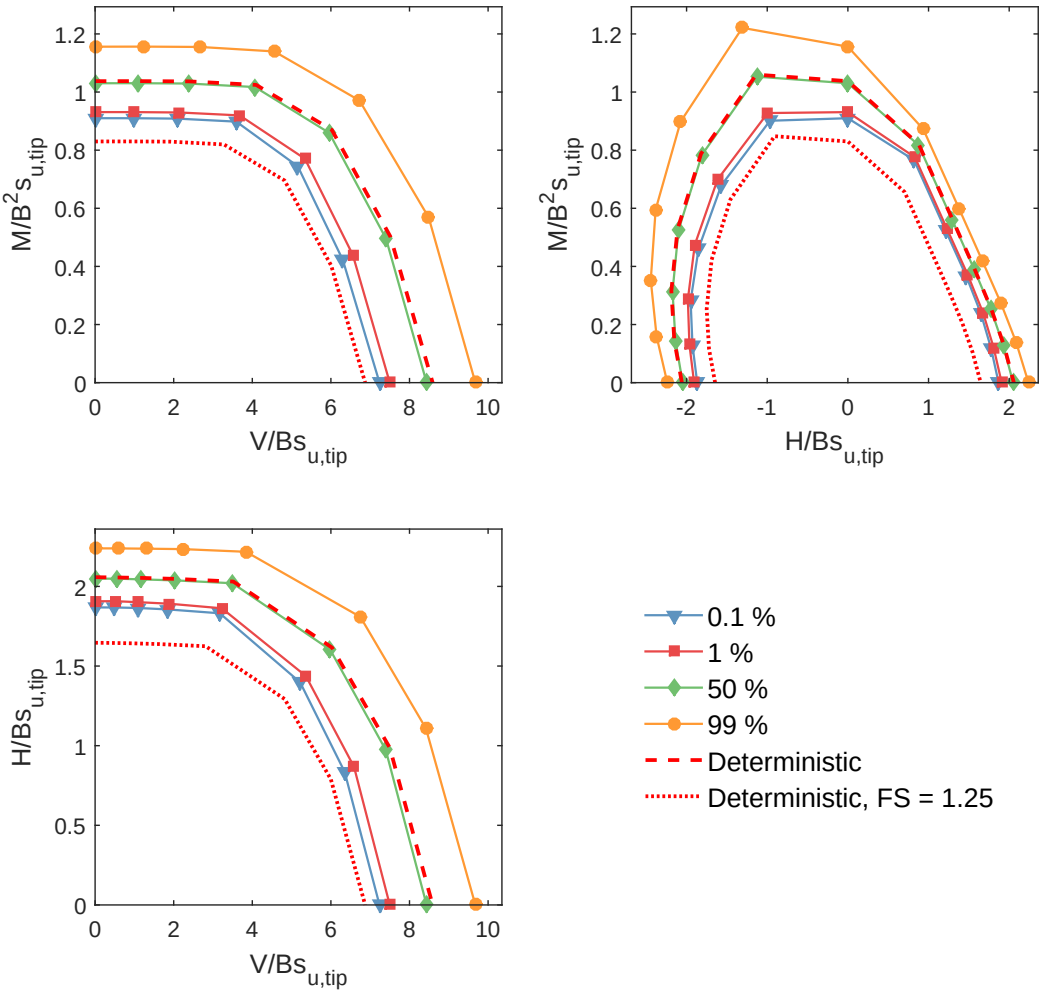

Figure 13: Probabilistic VHM failure envelopes for D/B = 0.25.

For embedment ratios greater than 0, the variability around the envelope is more consistent in the VM and VH planes than the HM plane. This is likely due to the fact that the transition between failure mechanisms is more straightforward. However, P_f^{FS} can be seen to approach 10^{-3} with increasing vertical load and actually exceeds the $\boldsymbol{N}_{\boldsymbol{c},0.1}$ envelope at D/B = 1. The vertical load component therefore has a critical influence on the probability of failure in a clay of increasing strength with depth.

The probabilistic failure envelopes offer a simple quantification of the uncertainty in ultimate capacity resulting from the natural spatial variability of a clay deposit. It is important to

note that the failure envelopes presented in this paper are applicable only to the soil conditions considered, which were chosen to be typical of an offshore scenario. Changes in either the deterministic soil properties or statistical characterisation of the soil, for example autocorrelation distance or COV, would alter the size and shape of the envelopes.

If a higher value of COV_{s_u} was considered, it is likely that the distance between the extreme envelopes, e.g. $\boldsymbol{N_c}_{,1}$ and $\boldsymbol{N_c}_{,99}$, would increase and lead to a greater probability of failure. Widening of the probabilistic envelopes under increasing COV was observed by Cassidy et al. [8] for strip footings under combined loading. Results from probabilistic studies of the vertical bearing capacity of strip footings have suggested that the vertical autocorrelation distance has more effect on the tails of the distribution than the horizontal distance [1]. A longer autocorrelation in the vertical direction would therefore be expected to have a similar effect on the probabilistic failure envelopes as an increase in COV. This emphasises the need to adequately characterise the statistical properties of the soil before using probabilistic methods in design. However, the observations made in this study regarding potential 'at-risk' areas of the failure envelope remain valid.

4. Conclusion

A probabilistic study of the ultimate capacity of skirted foundations in a spatially variable undrained clay has been carried out. The increase in undrained shear strength with depth commonly observed in marine clays was taken into account by a transformation of a homogeneous random field. Monte Carlo simulations employing an unmodified FE code were used to characterise the stochastic response, with the ultimate capacity of the foundation under combined loading being determined by load probes of fixed ratio.

Under uniaxial loading, the mean of the foundation capacity was found to be very similar to that obtained using a deterministic profile of s_u across all embedment ratios. However, the COV varied depending upon the applied load and skirt length. The variability of the clay increased with depth but deeper mechanisms did not necessarily lead to a greater COV due to the influence of the type of failure mechanism. The probability of failure with respect to a deterministic analysis was also analysed and if no factor of safety is considered, P_f is approximately 0.5. If the material factor recommended by the ISO [16] is used (FS = 1.25), the probability of failure reduces to less than 10^{-3} which is likely to represent an acceptable reliability.

The ultimate capacity of skirted foundations under combined loading was investigated by constructing probabilistic failure envelopes from the CDFs of each load probe. The probabil-

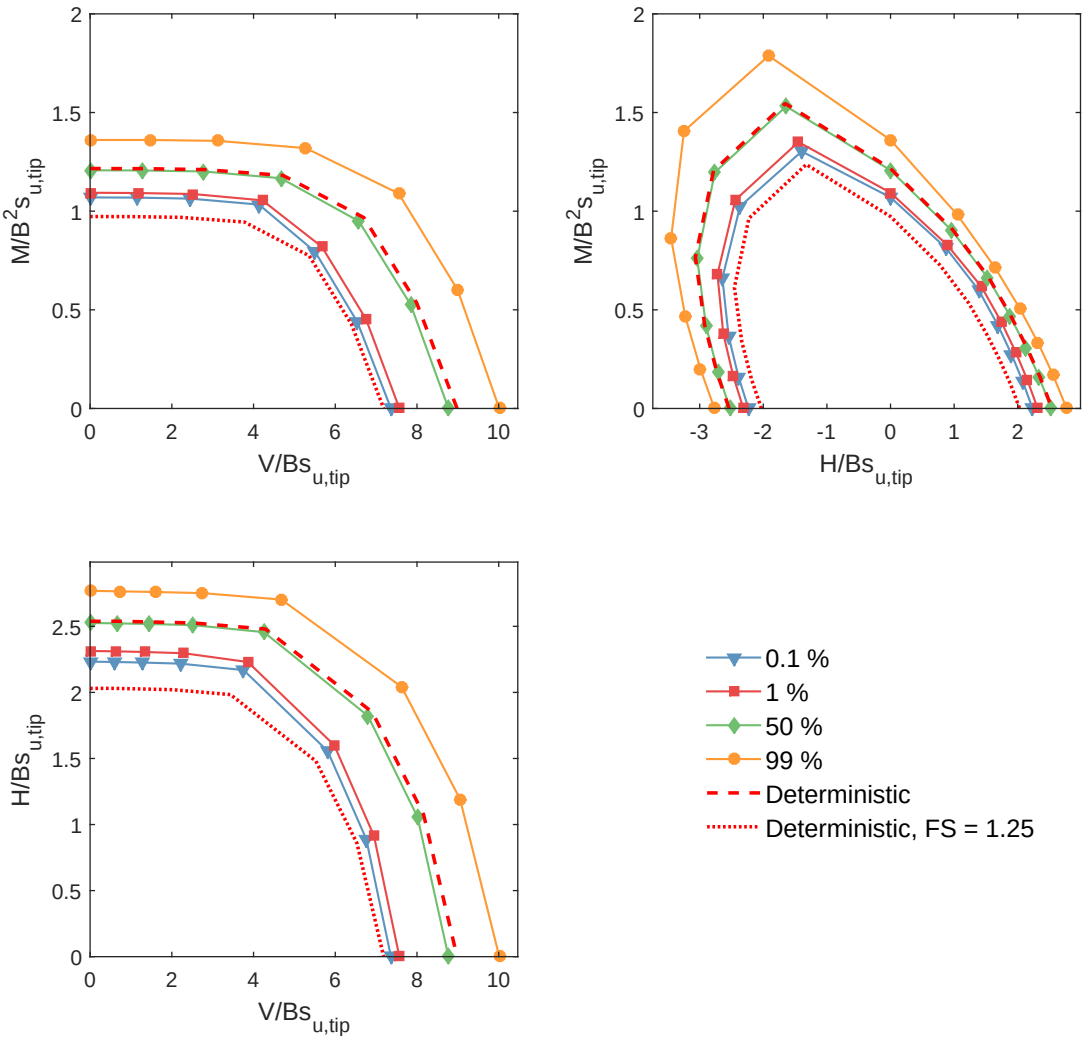

Figure 14: Probabilistic VHM failure envelopes for D/B = 0.5.

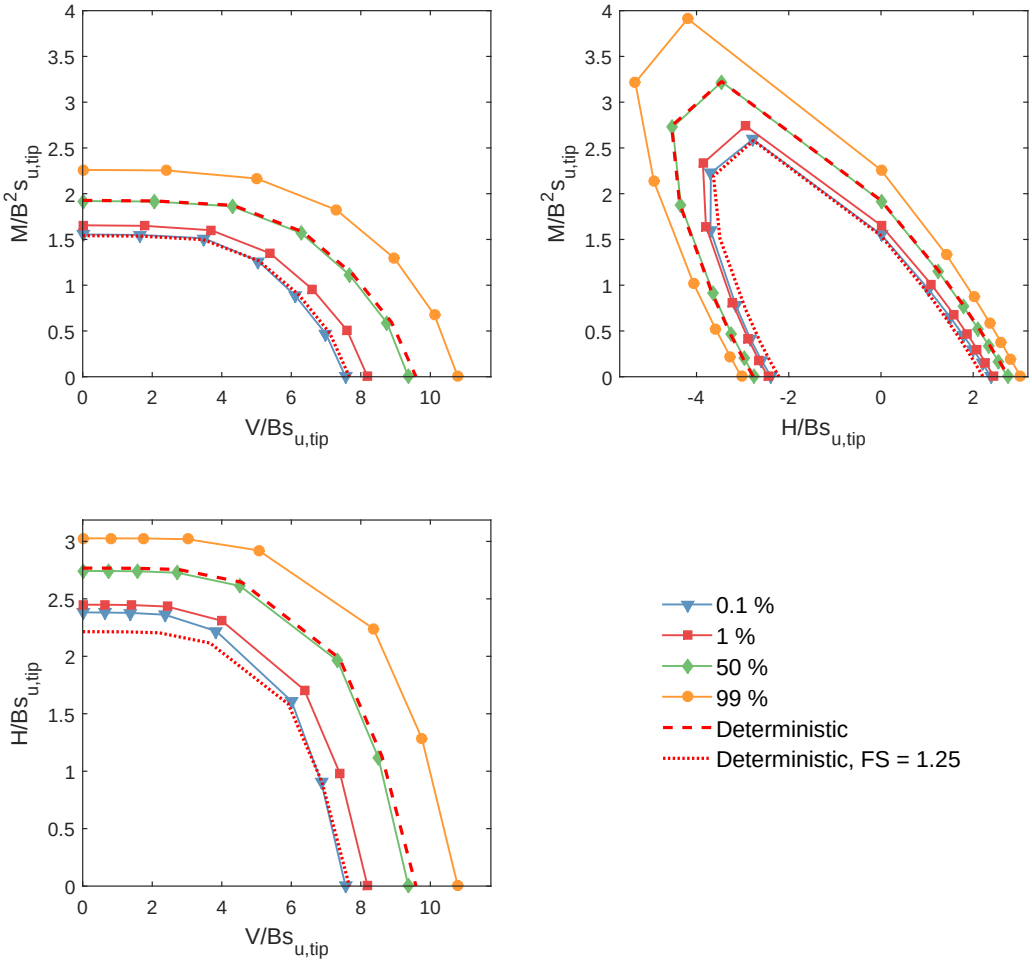

Figure 15: Probabilistic VHM failure envelopes for D/B = 1.

ity distribution of bearing capacity is not constant around the envelope, especially in the HM plane where the transition between failure mechanisms is particularly complex. The capacity of a skirted foundation under combined loading therefore cannot be adequately characterised in probabilistic terms from the uniaxial capacities alone. If the same factor of safety is applied as for the uniaxial load cases, the probability of failure is increased when the vertical load component is sufficient to affect bearing capacity and, in the HM plane, at peak moment capacity. This suggests that care should be taken in a failure envelope design approach if design loads approach these areas of the envelope.

The probabilistic failure envelopes presented here are limited to the specific case considered. However, the methodology demonstrates a straightforward and effective way of quantifying and understanding uncertainty in the ultimate limit state design of offshore geotechnical structures.

Reference

[1] Al-Bittar T, Soubra AH. Bearing capacity of strip footings on spatially random soils using sparse polynomial chaos expansion. Int J Numer Anal Methods Geomech, 2013; 37(13):2039-2060.

[2] Andersen KH, Murff JD, Randolph MF, Clukey EC, Erbrich C, Jostad HP, Hansen B, Aubeny CP, Sharma P, Supachawarote C. Suction anchors for deepwater applications. In: Proc Int Symp on Frontiers in Offshore Geotechnics (ISFOG), Perth, Western Australia, 2005; 3-30.

[3] Au S-K, Beck JL. Estimation of small failure probabilities in high dimensions by subset simulation. Probabilist Eng Mech, 2001; 16(4): 263-277.

[4] Blatman G, Sudret B. An adaptive algorithm to build up sparse polynomial chaos expansions for stochastic finite element analysis, Probablist Eng Mech; 2010, 25(2): 183-197.

[5] Botev ZI, Grotowski JF, Kroese DP. Kernel density estimation via diffusion. Ann Stat, 2010; 38(5):2916-2957.

[6] Bransby MF, Randolph MF. The effect of embedment depth on the undrained response of skirted foundations to combined loading. Soils Found, 1999; 39(4):19-34.

[7] Bransby MF, Yun G. The undrained capacity of skirted strip foundations under combined loading. Géotechnique, 2009; 59(2):115-125.

[8] Cassidy MJ, Uzielli M, Tian Y. Probabilistic combined loading failure envelopes of a strip footing on spatially variable soil. Comput Geotech, 2013; 49:191-205.

[9] Efron B. Bootstrap methods: another look at the jackknife. Ann Stat, 1979; 38(5):1-26.

[10] Ghanem RG, Spanos PD. Stochastic Finite Elements: A Spectral Approach. 2nd edn. New York: Dover Publications; 2003.

[11] Gourvenec S. Failure envelopes for offshore shallow foundations under general loading. Géotechnique, 2007; 57(9):715-728.

[12] Gourvenec S. Effect of embedment on the undrained capacity of shallow foundations under general loading. Géotechnique, 2008; 58(3):177-185.

[13] Gourvenec S, Barnett S. Undrained failure envelope for skirted foundations under general loading. Géotechnique, 2011; 61(3):263-270.

[14] Gourvenec S, Randolph M. Effect of strength non-homogeneity on the shape of failure envelopes for combined loading of strip and circular foundations on clay. Géotechnique, 2003; 53(6): 575-586.

[15] Griffiths DV, Fenton GA. Bearing capacity of spatially random soil: the undrained clay Prandtl problem revisited. Géotechnique, 2001; 51(4):351-359.

[16] ISO 19901-4:2003 Petroleum and natural gas industries - Specific requirements for offshore structures - Part 4: Geotechnical and foundation design considerations. Geneva: International Organization for Standardization, 2003.

[17] Keaveny JM, Nadim F, Lacasse, S. Autocorrelation functions for offshore geotechnical data. 5th Int Conf on Struct Saf and Reliability (ICOSSAR), San Francisco, 1989; 253-270.

[18] Lacasse S, Nadim F. Uncertainties in Characterising Soil Properties. Uncertainty in the geologic environment: from theory to practice. New York: ASCE; 1996:49-75.

[19] Li D-Q, Qi X-H, Phoon K-K, Zhang L-M, Zhou C-B. Effect of spatially variable shear strength parameters with linearly increasing mean trend on reliability of infinite slopes. Struct Saf, 2014; 49:45-55.

[20] Lumb P. The variability of natural soils. Can Geotech J, 1966; 3(2):74-97.

[21] Phoon KK. Reliability-based design in geotechnical engineering. London: Taylor & Francis; 2008.

[22] Phoon KK, Kulhawy FH. Characterization of geotechnical variability. Can Geotech J, 1999; 36(4):612-624.

[23] Pieczyńska-Kozłowska JM, Pula W, Griffiths DV, Fenton GA. Influence of embedment, self-weight and anisotropy on bearing capacity reliability using the random finite element method. Comput Geotech, 2015; 67(0): 229-238.

[24] Plaxis 2D. Delft, Netherlands: Plaxis bv; 2012.

[25] Popescu R, Deodatis G, Nobahar A. Effects of random heterogeneity of soil properties on bearing capacity. Probabilist Eng Mech, 2005; 20(4):324-341.

[26] Randolph, MF, Gaudin C, Gourvenec SM, White DJ, Boylan N, Cassidy MJ. Recent advances in offshore geotechnics for deep water oil and gas developments. Ocean Eng, 2011; 38(7):818-834.

[27] Randolph MF, Gourvenec S. Offshore geotechnical engineering. London: Spon Press; 2011.

[28] Ukritchon B, Whittle AJ, Sloan SW. Undrained limit analyses for combined loading of strip footings on clay. J Geotech Geoenviron Eng, 1998; 124(3):265-276.

[29] Vanmarcke, E. Random fields: analysis and synthesis. World Scientific; 2010.

[30] Wroth CP, Houlsby GT. Soil mechanics - property characterization and analysis procedures. Keynote Lecture. In: Proc 11th Int Conf on Soil Mechanics and Found Engng (ICSMFE), San Francisco; 1985:1-55.

[31] Wu S-H, Ou C-Y, Ching J, Juang CH. Reliability-based design for basal heave stability of deep excavations in spatially varying soils. J Geotech Geoenviron Eng 2012;138(5):594-603.

[32] Yun G, Bransby MF. The horizontal-moment capacity of embedded foundations in undrained soil. Can Geotech J, 2007; 44(4):409-424.

List of Tables

List of Figures